Honeywell

HONEYWELL INTERNATIONAL INC
PERFORMANCE MATERIALS & TECHNOLOGIES
115 Tabor Road
Morris Plains, NJ 07950 - USA
www.honeywell.com

November 18, 2019

Dr. Souad A. Benromdhane, Ph.D.
Office of Air Quality Planning and Standards
U.S. Environmental Protection Agency
Mail Code C539-07
Research Triangle Park, NC 27711

Dear Dr. Benromdhane,

In our last conversation you had asked Honeywell to provide an MIR report on CF_3I, in addition to the OH reactivity information submitted earlier. Dr. William Carter he kindly reviewed the data and provided a report on the ground-level atmospheric ozone formation potential of trifluoromethyl iodide. The completed report is attached. In this report, Dr. Carter has provided estimates of the potential of CF_3I to form ground-level atmospheric ozone under various atmospheric conditions scenarios representing different ozone reactivity scales, including the maximum incremental reactivity (MIR). As in previous cases, the results are compared with those of ethane.

In summary, Dr. Carter reports CF_3I to be an actual inhibitor for ozone formation under most atmospheric conditions where NO_x levels are favorable for ozone formation. For certain high NO_x levels, i.e. MIR conditions, CF_3I is estimated to promote ozone formation. However, he also makes several arguments as to whether the MIR scale results are appropriate to use for the evaluation of this compound, as described in the last section of this report titled "*Use of Reactivity Results for Exemptions*". Briefly the arguments made include:

- CF_3I reactivity results are sensitive to NO_x levels, i.e., only slight reductions of NO_x levels, below MIR, results in much lower or negative reactivities for CF_3I;
- The positive MIR reactivities were attributed to INO_2 formation, a temporary sink of NO_x, which in the long run inhibits ozone formation;
- The MIR reactivities represent only an upper limit due to literature discrepancies on INO_2 atmospheric decomposition rate; and
- The CF_3I reactivity behavior is very similar to 2-amino-2-methyl-1-propanol (AMP), a compound already exempted from VOC regulations. The similarity is due to the formation of strong NO_x sinks under MIR conditions in both chemical mechanisms.

In conclusion, the report by Dr. Carter suggests that CF_3I is an ozone inhibitor under most atmospheric conditions, and while under rare MIR conditions reactivity values exhibit those of ethane, reasonable arguments can be made to explain this behavior and justify a VOC exemption.

Sincerely,

Sandeep Mukhi

Sandeep Mukhi, Ph.D., DABT.
Director, Toxicology and Product Stewardship-Americas

ESTIMATION OF THE GROUND-LEVEL ATMOSPHERIC OZONE FORMATION POTENTIAL OF TRIFLUOROMETHYL IODIDE

Report to
Honeywell International Inc
October 31, 2019

By

William P. L. Carter
Research Chemist and Consultant
2284 Mt. Vernon Avenue,
Riverside, California 9207

Summary

Estimates of ground-level atmospheric ozone impacts in the MIR and other ozone reactivity scales have been calculated for the first time for trifluoromethyl iodide (CF_3I). The ozone impacts were calculated using the SAPRC-11 atmospheric chemical mechanism, with the mechanism for the iodides and trifluoromethyl radical reactions added. The newly developed mechanism for iodides reactions was tested against available environmental chamber experiments of methyl iodide (CH_3I) and it was found to represent the experimental data reasonably well. The CF_3I ozone reactivities were then calculated for various box model scenarios for conditions representing the MIR and other reactivity scales. The results are compared with those of ethane, which the EPA has used as an informal standard for determining exemptions for regulations of volatile organic compounds (VOCs) as ozone precursors.

CF_3I is predicted to be an ozone inhibitor under most atmospheric conditions where NO_x levels are favorable for ozone formation, but to have positive effects on ozone formation under high NO_x, maximum incremental reactivity (MIR) conditions where ozone is most sensitive to reactive VOC emissions. The MIR reactivities of CF_3I were either ~3 times higher or within the variabilities of the reactivities of ethane, depending on what is assumed about the uncertain cross-sections of INO_2, for which there is a discrepancy in the literature. However, only slight reductions of NO_x levels below MIR results in much lower or negative reactivities for CF_3I, making it an inhibitor for most atmospheric conditions. The positive values for the MIR reactivities were attributed to NO_x sinks caused by INO_2 formation, which in the long run inhibit ozone formation. These reactivity characteristics are similar to those observed previously for 2-amino-2-methyl-1-propanol (AMP), which the EPA has already exempted.

Contents

Introduction

Ozone in photochemical smog is formed from the gas-phase reactions of volatile organic compounds (VOCs) and oxides of nitrogen (NO_x) in sunlight, and control of both VOCs and NO_x is required to attain air quality standards for ozone. Many different types of VOCs are emitted into the atmosphere, each reacting at different rates and having different mechanisms for their reactions. Because of this, they can differ significantly in their effects on ozone formation, or their "reactivity". In recognition of this, the U.S. EPA has exempted volatile organic certain compounds with ozone impacts expected to be less than ethane from regulations as VOC ozone precursors (Dimitriades, 1999; RRWG, 1999a, EPA 2005), and the California Air Resources Board (CARB) has adopted regulations with reactivity-based adjustments for several types of VOC sources (CARB 1993, 2000, 2016).

Use of reactivity-based regulations for VOCs require some means to quantify ozone impacts for VOCs. The approach that is generally adopted is to use the "incremental reactivity" of the VOC, which is the change in ozone caused by adding a small amount of the VOC to the emissions in an ozone pollution episode, divided by the amount of VOC added (Carter, 1994a; Dimitriades, 1999; RRWG 1999a,b). It is important to recognize that incremental reactivities depend on both the VOC and the episode where it is emitted, and for atmospheric conditions they must be calculated using computer airshed models using models for the airshed conditions and chemical mechanisms for the atmospheric reactions involved in ground-level ozone formation (Carter, 1994a; RRWG, 1999b). Different ozone reactivity scales can be developed to represent different types of environmental conditions, ozone quantification methods, or models for airshed conditions (Carter, 1994a, RRWG 1999b; Carter et al, 2003), but the most widely used scale is the Maximum Incremental Reactivity (MIR) scale of Carter (1994a). This scale, which has undergone a number of updates using updated chemical mechanisms (Carter, 2000, 2016), is used in the CARB's current reactivity-based regulations. Ozone impacts in other scales are also considered when determining reactivity relative to ethane when the EPA makes VOC exemption decisions.

Trifluoromethyl iodide (CF_3I) is a compound of interest to Honeywell International Inc., and its use and manufacture may result in it being emitted into the atmosphere, where it may be subject to VOC regulations aimed at reducing ozone formation. At present no ozone impact estimates are available for this compound, though there are data concerning its atmospheric photolysis, which is expected to be its only atmospheric reaction. The photolysis is sufficiently rapid that the compound should have non-negligible impacts on atmospheric reactions, and is faster to the photolysis of methyl iodide (CH_3I),

whose ozone impacts we have studied previously (Carter, 2007). In our previous study we calculated that methyl iodide had negative impacts on ozone formation under most conditions, and as a result the EPA has granted it an exemption from regulation as a VOC ozone precursor (EPA, 2019). Although both CH_3I and CF_3I both form iodine atoms whose reactions cause ozone destruction, it was unclear how replacing $CH_3\cdot$ with $CF_3\cdot$ would affect atmospheric ozone impacts.

To address this, in this report we discuss a derivation of the atmospheric reaction mechanism for CF_3I, including the reactions of the $CF_3\cdot$ radicals and iodine atoms formed in the photolysis reactions. As part of this work, we updated the iodine reaction mechanism we previously derived for methyl iodide and re-evaluated the revised mechanism against available chamber data we used to evaluate the previous mechanism for CH_3I (Carter et al, 2007). The reactivity results for these iodides are then compared with reactivity results already derived for ethane.

Methods

Base Chemical Mechanism Used

The chemical mechanism used to derive the reactivity scales used in the current CARB reactivity based regulations is the SAPRC-07 mechanism of Carter (2010a,b), That mechanism has since been updated to SAPRC-11 (Carter and Heo, 2012, 2013), though the update affected primarily aromatics and did not cause significant changes in reactivities for most other compounds (Carter, 2010). Even though the regulatory reactivity scale has not been updated to SAPRC-11, this is used as the basis of the reactivity estimates for this work. Although that there is an updated version of SAPRC being developed and a preliminary version has been used in some exploratory airshed calculations (Venecek et al, 2018), it is not yet ready for use in deriving reactivity scales. Since the main objective is to estimate the reactivities relative to ethane, and since the ethane mechanism has not been modified since SAPRC-07 was developed, the reactivities calculated relative to ethane should not change with the mechanism update, as long as the mechanisms for the compounds of interest have not been modified.

Briefly, the SAPRC mechanisms consists of two major components: the "base" mechanism that is used to represent the full set of VOC emissions from all sources, and the specific mechanisms for the individual VOCs whose ozone impacts were assessed. The individual VOCs whose incremental reactivity are calculated are represented explicitly, while most of the other VOCs that are emitted into the ozone scenario being modeled are represented using lumped model species in the base mechanism. See Carter (2010a,b) and Carter and Heo (2013) for a more complete discussion of how the SAPRC-07 and SAPRC-11 are used to represent the various VOCs in reactivity assessment calculations. A complete listing of the mechanism employed is given by Carter and Heo (2013), though some minor corrections have been made since there. The mechanism as used in this work can be downloaded from the SAPRC mechanism web site (Carter, 2013). Note that the downloadable mechanism does not include the iodide and $CF_3\cdot$ reactions developed in this work.

Atmospheric Reactions of Methyl and Trifluoromethyl Iodide

Although this work focuses on the atmospheric impacts of CF_3I, we will also discuss the mechanism for CH_3I because it forms the same iodine species, and because there are environmental chamber data available to test mechanisms developed for the reactions of these species (Carter et al, 2007). Although ideally there should be chamber data to directly evaluate mechanisms developed for CF_3I, the most uncertain portion of the mechanism concerns the reactions of the iodine atoms and the iodine oxides they form, and data for CH_3I can test at least this portion of the mechanism.

The major atmospheric consumption reaction for CH_3I and CF_3I is photolysis to form iodine atoms and methyl or trifluoromethyl radicals.

$$CF_3I + h\nu \rightarrow CF_3\cdot + I\cdot \quad (1)$$
$$CF_3\cdot + O_2 \rightarrow CF_3OO\cdot \quad (2)$$
$$CF_3OO\cdot + NO \rightarrow NO_2 + CF_3O\cdot \quad (3)$$
$$CF_3O\cdot + NO_2\ (+ M) \rightarrow CF_3ONO_2\ (+ M) \quad (4)$$
$$CF_3O\cdot + \text{organics} \rightarrow CF_3OH + \text{other products (including radicals)} \quad (5)$$

$$CH_3I + h\nu \rightarrow CH_3\cdot + I\cdot \quad (6)$$
$$CH_3\cdot + O_2 \rightarrow CH_3OO\cdot \quad \text{(incorporated in base mechanism)}$$
$$CH_3OO\cdot + NO \rightarrow NO_2 + CH_3O\cdot \quad \text{(incorporated in base mechanism)}$$
$$CH_3O\cdot + O_2 \rightarrow HCHO + HO_2\cdot \quad \text{(incorporated in base mechanism)}$$

For direct overhead sun, CH_3I is calculated to have a half life of ~1 day with respect to photolysis, while CF_3I is calculated to photolyze about 4 times faster, with a half life of ~6 hours (see Table 2, below). Methyl iodide also reacts with OH radicals, as shown below. There is no analogous reaction for CF_3I.

$$CH_3I + OH \rightarrow H_2O + ICH_2\cdot \quad (7)$$
$$ICH_2\cdot + O_2 \rightarrow ICH_2OO\cdot \quad (8)$$
$$ICH_2OO\cdot + NO \rightarrow NO_2 + ICH_2O\cdot \quad (8)$$
$$ICH_2O\cdot \rightarrow HCHO + I\cdot \quad (10)$$

The base mechanism used (discussed above) already includes representations for reactions of the methyl radicals and formaldehyde formed from methyl iodide, but does not include reactions of iodine atoms formed from both and the $CF_3\cdot$ radicals formed from CF_3I. A mechanism for I atoms was derived previously (Carter et al, 2007) but was updated for this work. No mechanism was previously derived for $CF_3\cdot$, so this is done as part of this project.

Table 1 gives a listing of the reactions and rate constants added to the SAPRC-11 mechanism to represent the reactions of methyl and trifluoromethyl iodide and the radicals and other reactive intermediates formed in their reactions. Most model species whose reactions are listed on Table 1 represent individual compounds explicitly, and it is obvious from their names which compounds they represent. The exceptions are (1) "RO2C", which represents an NO to NO_2 conversion caused by reactions of peroxy radicals; (2) "xHCHO", which represents formation of formaldehyde following reactions of peroxy radicals with NO; and (3) "PM-I", which represents an iodine atom in a non-volatile iodine oxide

A number of updates and corrections were made to the mechanisms of the iodine species relative to the iodine mechanism used previously for CH_3I (Carter, 2007). Many of the rate constants were updated to the NASA (2015) recommendations, the iodine oxide reactions were updated based primarily on the mechanism for the iodine oxides derived by Gómez Martín et al (2013), and the iodine oxide absorption cross sections of Saiz-Lopez et al (2014). In addition, estimated absorption cross sections for INO_2 used previously were replaced by directly measured values for this compound, and the error in the input file for the reactions of CH_3I with OH was corrected (see note 1 on Table 1).

The $CF_3\cdot$ radicals formed in the photolysis of CF_3I are expected to react in the presence of NO_x in air to form $CF_3O\cdot$, which is not represented in the base mechanism. It is unlike essentially all other alkoxy radicals formed in the atmospheric in that it has no non-negligible unimolecular reactions and it does not react with O_2, so its only significant atmospheric reactions is reactions with NO_x, other radicals, or (like OH but unlike other organic alkoxy radicals) with VOCs. Other alkoxy radicals may also react with VOCs with relatively high rate constants, but these bimolecular reactions are negligible loss processes

Table 1. List of reactions and rate constants added to the SAPRC-11 mechanism to represent the reactions of methyl and trifluoromethyl iodides.

Reaction and Products [a]	Rate Parameters [b] k(300)	A	Ea	B	Notes [c]
Reactions of methyl and trifluoromethyl iodide					
CH3I + OH = RO2C + xHCHO + I	1.03e-13	4.30e-12	2.23		1
CH3I + HV = MEO2 + I	Phot Set= CH3I				1
CF3I + HV = CF3O2 + I	Phot Set= CF3I				2
Reactions of Iodine Species					
I + O3 = IO + O2	1.27e-12	2.30e-11	2.73		2
I + HO2 = HI + O2	3.96e-13	2.50e-11	2.17		2
HI + HV = HO2 + I	Phot Set= HI				2
I + NO = INO	INO formation ignored because of				
INO + HV = I + NO	slow formation and rapid photolysis				
I + NO2 = INO2	4.83e-12	Falloff, F=0.60, N=2.20			2
	0:	3.00e-31	0.00	-2.00	
	inf:	6.60e-11	0.00	0.00	
INO2 + HV = I + NO2	Phot Set= INO2 (varied -- see text)				2, 3
I + NO3 = IO + NO2	1.00e-10				4
IO + HO2 = HOI + O2	8.69e-11	2.30e-11	-2.13		2
HOI + HV = OH + I	Phot Set= HOI-JPL				2
IO + NO = I + NO2	2.03e-11	9.10e-12	-0.48		2
IO + IO = #.13 {I + I + O2} + #.33 {I + OIO} + #.54 I2O2	9.84e-11	5.40e-11	-0.36		5
IO + O3 = O2 + OIO	5.00e-16				6
IO + OIO = I2O3	4.20e-11				7
IO + NO = IONO	IONO formation ignored because of				
IONO + HV = IO + NO	rapid reversal by IONO photolysis				
IO + NO2 = IONO2	3.36e-12	Falloff, F=0.60, N=2.30			2
	0:	7.50e-31	0.00	-2.50	
	inf:	7.60e-12	0.00	-3.50	
IONO2 = IO + NO2	Same as k(PAN decomposition)				8
IONO2 + HV = I + NO3	Phot Set= IONO2				2
OIO + OIO = I2O4	1.70e-11				7
OIO + HV = I + O2	Phot Set= OIO, qy= 0				9
I2O2 + O3 = O2 + I2O3	5.00e-16				10
I2O3 + O3 = I2O4 + O2	5.00e-16				7
I2O4 + O3 = I2O5 + O2	5.00e-16				7
I2O4 + IO = I3O5	1.50e-11				7
I2O4 + OIO = I3O6	2.80e-12				7
I2O5 + OIO = I3O7	1.00e-13				7
I2O2 = I + OIO	1.20e-3				7

Table 1 (continued)

Reaction and Products [a]	Rate Parameters [b] k(300)	A	Ea	B	Notes [c]
I2O4 = OIO + OIO	1.10e-2				7
I3O5 = I2O4 + IO	6.20e+4				7
I3O6 = I2O4 + OIO	3.50e+4				7
I3O7 = I2O5 + OIO	3.70e+7				7
I2O3 + I2O3 = #4 PM-I	1.40e-12				7, 11
I2O3 + I2O4 = #4 PM-I	2.70e-11				7, 11
I2O4 + I2O4 = #4 PM-I	2.70e-10				7, 11
I2O4 + I2O5 = #4 PM-I	1.20e-11				7, 11
I2O5 + I2O5 = #4 PM-I	7.00e-11				7, 11
I2O2 + HV = I + OIO	Phot Set= I2O2				12
I2O3 + HV = IO + OIO	Phot Set= I2O3				12
I2O4 + HV = OIO + OIO	Phot Set= I2O4				12
Reactions of trifluoromethyl species					
CF3O2 + NO = NO2 + CF3O	Same as k(RO2+NO)				13
CF3O2 + NO3 = NO2 + CF3O	Same as k(RO2+NO3)				13
CF3O2 + HO2 = CF3OOH + O2	Same as k(RO2+HO2)				13
CF3OOH + HV = CF3O + OH	Phot Set= COOH				13, 14
CF3O + O3 = CF3O2 + O2	1.88e-14	2.00e-12	2.78		2
CF3O + NO2 = CF3ONO2	9.64e-12	Falloff, F=0.60, N=2.50			2
	0:	2.70e-28	0.00	-6.90	
	inf:	2.10e-11	0.00	-2.00	
CF3ONO2 + HV = CF3O + NO2					15
CF3O + CH4 = CF3OOH + MEO2	2.29e-14	2.60e-12	2.82		2
CF3O + organics = products [+ CF3OH if abstraction]	k = 3.57 x k(VOC+OH)				16

[a] Format of reaction listing: "=" separates reactants from products; "#*number*" indicates stoichiometric coefficient, "#*coefficient* {*product list*}" means that the stoichiometric coefficient is applied to all the products listed.

[b] Except as indicated, the rate constants are given by $k(T) = A \cdot (T/300)^{B} \cdot e^{-Ea/RT}$, where the units of k and A are cm^3 $molec^{-1}$ s^{-1} if bimolecular, or s^{-1} if unimolecular, Ea are kcal mol^{-1}, T is ^oK, and R=0.0019872 kcal mol^{-1} deg^{-1}. The following special rate constant expressions are used:

Phot Set = *name*: The absorption cross sections for the photolysis reactions are given in Table 3. The photolysis rate constants for direct overhead sunlight as used in the reactivity calculations are given on Table 2. Unit quantum yields are assumed unless noted otherwise.

Falloff: The rate constant as a function of temperature and pressure is calculated using $k(T,M) = \{k0(T)\cdot[M]/[1 + k0(T)\cdot[M]/kinf(T)]\}\cdot F^{Z}$, where $Z = \{1 + [\log10\{k0(T)\cdot[M])/kinf(T)\}/N]^2\}^{-1}$, [M] is the total pressure in molecules cm^{-3}, F and N are as indicated on the table, and the temperature dependences of k0 and kinf are as indicated on the table.

Same as k(x): Rate constant assumed to be the same as used for the reaction x.

[c] Footnotes documenting sources of rate constants and mechanisms are as follows.

1 The absorption cross sections and OH radical rate constants are as recommended by IUPAC (2019) (Sheet oIOx1, dated June, 2015, for photolysis and Sheet PI8, dated December, 2000, for

Table 1 (continued)

the OH reaction). These are the same used by Carter (2007). The mechanisms are based on the overall processes as shown in the text as Reactions (7) through (10), where MEO2 represents methyl peroxy radicals (which are explicit in SAPRC-11) and RO2R + xHCHO represents the formation of formaldehyde after an NO to NO_2 conversion in the base SAPRC-11 mechanism. This mechanism is the same as tabulated by Carter (2007), but the input file used in the reported calculations erroneously had HO_2 also being formed in this reaction. This was found not have a large impact on the calculations because most of the CH_3I reacts by photolysis, but is corrected in this work.

2 As recommended by NASA (2015)

3 The absorption cross sections given in Table 3 are based on NASA (2015) recommendations. However, there is a factor of 2.48 discrepancy between the NASA recommended absorption cross sections (which in turn are based on a earlier IUPAC [2000] evaluation) for INO_2 and those on the Maintz database attributed to the thesis of Bröske (2000), which is apparently the only experimental measurement considered in the evaluations. The NASA (2015) write-up notes the discrepancy in the Mainz database but adopts the IUPAC evaluation without comment. The IUPAC write-up does not state why the reported values are different than those on the Mainz database for Bröske (2000), but does say that the values are preliminary because the write-up and analysis was not completed at that time, which was also 2000. They cited a 1999 version of the Bröske thesis, which is presumably superceded by Bröske (2000). Therefore, it is not clear why there is a factor of 2.5 difference, and it could be that the actual photolysis rate is 2.5 times faster. It could be that Bröske found some reason to change the calibration factor after the IUPAC review was completed but before he submitted the results to the Mainz database. As discussed in the text the absorption cross sections are important in affecting incremental reactivity under high NO_x conditions, so calculations are done using both the NASA and IUPAC recommended absorption cross sections and also the cross sections of Bröske (2000) from the Mainz database.

4 This reaction is omitted in the NASA (2015) evaluation. The rate constant used is as recommended by IUPAC (2019) (sheet iIOX7, dated June, 2008).

5 Products and rate constants are based on the current IUPAC (2019) evaluation (sheet iIOx17, dated Feb, 2004), which preferred the data of Bloss et al (2001). They reported yields of 11%, 28% and 46% for formation of I+I+O2, I+OIO, and I2O2, respectively. These are normalized to yield 13%, 33%, and 54%, respectively.

6 This is the limit value from Dillon et al (2006) as used by Gomez Martin et al (2013). The actual rate constant could be lower, but the reaction was relatively unimportant in accounting for O_3 loss from iodine species, so the effect of this uncertainty was not examined.

7 Mechanism taken from Gomez Martin et al (2013). Reactions found to be negligible are excluded.

8 Assumed to decompose with a similar rate constant as assumed for PAN ($CH_3C(O)OONO_2$). This is highly uncertain, but the thermal decomposition of $IONO_2$ is estimated to be unimportant compared to photolysis, so the effect of this uncertainty was not examined.

9 Absorption cross sections of Spietz et al (2005) taken from the Mainz spectral database (Keller-Rudek et al, 2013). The NASA (2015) recommended absorption cross sections could not be used because they do not give data for the full wavelength range that needs to calculate atmospheric photolysis rates. Tucceri et al (2006) found no evidence for I atom formation at 560-580 nm, and established upper limits of 5% for this range and 24% for 523 nm. We assume that the quantum yields for photodecomposition are low, but this is an area of uncertainty. Sensitivity calculations indicate that assuming a nonzero quantum yield does not affect MIR predictions, though it has an effect on the amount of inhibition predicted for low NO_x conditions.

Table 1 (continued)

10 This reaction was omitted from Gomez Martin et al (2013). It is assumed to have the same rate constant as used for IO + O_3 and I_2O_3 + O_3.

11 The higher iodine oxide species formed in these reactions are assumed to condense into the particle phase. Iodine atoms in the particle phase are represented by the unreactive counter species "PM-I". This could be used to estimate effects of the iodides on particle formation, which is beyond the scope of the present project.

12 Absorption cross sections were derived from Table 1 of Saiz-Lopez et al (2014) and references therein.

13 Assumed to react with same rate constants as assigned for analogous reactions of lumped peroxy radicals or alkyl hydroperoxides.

14 Methyl hydroperoxide photolysis rates are used to approximate that for trifluoromethyl hydroperoxide.

15 Assumed to photolyze with comparable rate as alkyl nitrates. Absorption cross sections of isopropyl nitrate is used for these compounds.

16 One reaction with $CF_3O\cdot$ was added for all model species in the mechanism that represent reactive organic compounds. The rate constants were estimated using Equation (I), as discussed in the text. The products are assumed to be the same as those formed in the OH reaction, with H_2O replaced by CF_3OH for abstraction reactions. See Carter and Heo (2013) for a list and descriptions of these model species and for the products they form. No attempt was made to determine which reactions were the most important or could be neglected.

Table 2. Photolysis rate constants for photolysis reactions listed in Table 1.

Phot File Name	Z=0 Phot k (min^{-1}) [a]	Comments and sources of absorption cross sections
CH3I	5.2e-4	From NASA (2015)
CF3I	2.2e-3	From NASA (2015)
NO2-06	0.72	The NO_2 photolysis rate is shown for comparison. Part of base mechanism
COOH	3.9e-4	Used for hydroperoxides. Part of base mechanism
IC3ONO2	2.4e-4	Used for organic nitrates. Part of base mechanism
OIO	< 35.6 (0 used)	Spietz et al (2005); Keller-Rudek et al (2013). Upper limit is derived assuming unit quantum yields, but the actual quantum yields are estimated to be very low. Therefore, this photolysis was not used in the model.
I2O2	4.7	From Saiz-Lopez et al (2014) and references therein.
I2O3	44.7	From Saiz-Lopez et al (2014) and references therein.
I2O4	15.4	From Saiz-Lopez et al (2014) and references therein.
INO2	0.22 0.50 5.7	Standard model. Based on IUPAC (2000) and NASA (2015) recommendations. Higher INO_2 photolysis reported by Bröske (2000) Very fast INO_2 photolysis as used by Carter (2007)
IONO2	3.7	From NASA (2015)

[a] Photolysis rate constant calculated using the light model used to calculate the photolysis rates for the reactivity scenarios (Carter, 1994, 2010a), for direct overhead sun (Zenith angle = 0).

Table 3. Absorption cross section data for photolysis reactions used in the methyl and trifluoromethyl iodide mechanisms. First number is wavelength in nm, the second is the absorption cross sections in cm^{-2}. Unit quantum yields assumed for all these reactions unless noted differently in the text.

---- CH3I ----									
205	7.00e-20	300	8.62E-20	265	9.96E-19	326	2.99E-19	426	1.99E-19
210	3.80e-20	305	4.99E-20	270	8.71E-19	328	3.22E-19	428	1.82E-19
215	5.20e-20	310	2.83E-20	275	8.98E-19	330	3.43E-19	430	1.66E-19
220	6.90e-20	315	1.57E-20	280	9.96E-19	332	3.61E-19	432	1.50E-19
225	9.10e-20	320	8.61E-21	285	9.22E-19	334	3.76E-19	434	1.34E-19
230	1.26e-19	325	4.49E-21	290	8.10E-19	336	3.85E-19	436	1.19E-19
235	2.02e-19	330	2.48E-21	295	6.20E-19	338	3.91E-19	438	1.06E-19
240	3.74e-19	335	1.33E-21	300	3.73E-19	340	3.92E-19	440	9.30E-20
245	6.36e-19	340	7.14E-22	305	3.08E-19	342	3.89E-19	442	8.10E-20
250	9.21e-19	345	3.80E-22	310	2.47E-19	344	3.82E-19	444	7.03E-20
255	1.11e-18	350	2.08E-22	315	2.51E-19	346	3.71E-19	446	6.05E-20
260	1.12e-18	355	1.15E-22	320	2.75E-19	348	3.56E-19	448	5.17E-20
265	9.66e-19	360	6.40E-23	325	3.25E-19	350	3.39E-19	450	4.40E-20
270	7.17e-19	365	3.60E-23	330	3.12E-19	352	3.20E-19	452	3.72E-20
275	4.71e-19	370	2.00E-23	335	3.49E-19	354	3.01E-19	454	3.13E-20
280	2.80e-19	375	1.10E-23	340	3.73E-19	356	2.80E-19	456	2.61E-20
285	1.52e-19	380	7.00E-24	345	3.73E-19	358	2.60E-19	458	2.17E-20
290	7.79e-20	385	4.00E-24	350	2.98E-19	360	2.41E-19	460	1.79E-20
295	3.92e-20	390	1.00E-24	355	2.95E-19	362	2.24E-19	462	1.47E-20
300	2.03e-20	395	00E+00	360	2.71E-19	364	2.08E-19	464	1.20E-20
305	1.09e-20			365	2.07E-19	366	1.95E-19	466	9.73E-21
310	6.19e-21	---- HI ----		370	1.49E-19	368	1.85E-19	468	7.85E-21
315	3.56e-21	275	1.24e-19	375	7.40E-20	370	1.78E-19	470	6.32E-21
320	2.15e-21	280	8.94e-20	380	2.40E-20	372	1.74E-19	472	5.05E-21
325	1.24e-21	285	6.37e-20	382	0	374	1.73E-19	474	4.02E-21
330	7.00e-22	290	4.51e-20			376	1.75E-19	476	3.18E-21
335	3.30e-22	295	3.17e-20	---- HOI-JPL ----		378	1.80E-19	478	2.50E-21
340	2.30e-22	300	2.23e-20	280	7.70E-22	380	1.88E-19	480	1.96E-21
345	1.27e-22	305	1.52e-20	282	1.21E-21	382	1.97E-19	485	00E+00
350	6.70e-23	310	1.01e-20	284	1.86E-21	384	2.08E-19		
355	2.60e-23	315	6.53e-21	286	2.81E-21	386	2.21E-19	---- IONO2 ----	
360	1.30e-23	320	4.09e-21	288	4.17E-21	388	2.34E-19	245	1.21E-17
365	4.00e-24	325	2.47e-21	290	6.08E-21	390	2.48E-19	250	1.17E-17
367	00e+00	330	1.45e-21	292	8.67E-21	392	2.61E-19	255	1.06E-17
		335	8.30e-22	294	1.22E-20	394	2.73E-19	260	9.46E-18
		340	4.70e-22	296	1.68E-20	396	2.84E-19	265	8.80E-18
---- CF3I ----		347	00e+00	298	2.27E-20	398	2.94E-19	270	7.97E-18
235	7.49E-20			300	3.02E-20	400	3.01E-19	275	7.72E-18
240	1.27E-19	---- INO2 ----		302	3.95E-20	402	3.06E-19	280	7.41E-18
245	2.04E-19	210	2.36E-18	304	5.09E-20	404	3.09E-19	285	6.91E-18
250	3.08E-19	215	1.87E-18	306	6.44E-20	406	3.09E-19	290	6.31E-18
255	4.27E-19	220	1.96E-18	308	8.03E-20	408	3.07E-19	295	5.77E-18
260	5.30E-19	225	2.79E-18	310	9.85E-20	410	3.02E-19	300	5.25E-18
265	5.89E-19	230	3.47E-18	312	1.19E-19	412	2.95E-19	305	4.95E-18
270	5.87E-19	235	3.99E-18	314	1.42E-19	414	2.85E-19	310	4.62E-18
275	5.26E-19	240	4.22E-18	316	1.66E-19	416	2.74E-19	315	4.41E-18
280	4.29E-19	245	4.00E-18	318	1.92E-19	418	2.61E-19	320	4.04E-18
285	3.19E-19	250	3.30E-18	320	2.19E-19	420	2.47E-19	325	3.96E-18
290	2.19E-19	255	2.34E-18	322	2.46E-19	422	2.31E-19	330	3.80E-18
295	1.42E-19	260	1.62E-18	324	2.73E-19	424	2.15E-19	335	3.74E-18

Table 3 (continued)

340	3.60E-18			385	1.77E-17	340	1.58E-17	320	1.37E-21
345	3.48E-18	---- I2O3 ----		387	1.78E-17	344	1.54E-17	325	1.05E-21
350	3.34E-18	300	2.42E-17	388	1.78E-17	346	1.52E-17	330	7.90E-22
355	3.16E-18	301	2.42E-17	390	1.75E-17	349	1.52E-17	335	6.10E-22
360	2.94E-18	302	2.41E-17	391	1.72E-17	353	1.52E-17	340	4.70E-22
365	2.70E-18	304	2.39E-17	392	1.74E-17	355	1.50E-17	345	3.50E-22
370	2.42E-18	305	2.38E-17	394	1.74E-17	358	1.48E-17	350	2.70E-22
375	2.13E-18	306	2.37E-17	396	1.70E-17	360	1.49E-17	355	2.10E-22
380	1.84E-18	308	2.36E-17	398	1.69E-17	362	1.46E-17	360	1.60E-22
385	1.53E-18	309	2.35E-17	400	1.67E-17	366	1.44E-17	365	1.20E-22
390	1.30E-18	311	2.35E-17	401	1.64E-17	368	1.41E-17	370	0
395	1.03E-18	312	2.34E-17	402	1.66E-17	371	1.37E-17		
400	7.80E-19	314	2.32E-17	406	1.64E-17	374	1.32E-17	---- IC3ONO2 ----	
405	6.05E-19	317	2.30E-17	407	1.60E-17	377	1.26E-17	185	1.79E-17
440	0	319	2.29E-17	409	1.61E-17	378	1.21E-17	188	1.81E-17
		321	2.27E-17	411	1.57E-17	380	1.14E-17	190	1.79E-17
---- OIO ----		323	2.26E-17	414	1.53E-17	382	1.11E-17	195	1.61E-17
See note [a]		325	2.25E-17	416	1.54E-17	385	1.01E-17	200	1.26E-17
		328	2.23E-17	419	1.51E-17	386	8.56E-18	205	8.67E-18
---- I2O2 ----		330	2.22E-17	421	1.46E-17	388	7.31E-18	210	4.98E-18
306	2.80E-17	332	2.20E-17	424	1.43E-17	389	6.97E-18	215	2.47E-18
308	2.78E-17	334	2.20E-17	425	1.38E-17	390	5.19E-18	220	1.17E-18
309	2.77E-17	335	2.17E-17	427	1.37E-17	392	0	225	5.80E-19
311	2.75E-17	337	2.16E-17	430	1.29E-17			230	3.10E-19
313	2.72E-17	340	2.13E-17	433	1.25E-17	---- COOH ----		235	1.80E-19
314	2.69E-17	342	2.13E-17	435	1.16E-17	210	3.12E-19	240	1.10E-19
315	2.66E-17	344	2.10E-17	450	0	215	2.09E-19	245	7.00E-20
316	2.62E-17	346	2.09E-17			220	1.54E-19	250	5.70E-20
317	2.59E-17	348	2.08E-17	---- I2O4 ----		225	1.22E-19	255	5.20E-20
319	2.55E-17	350	2.06E-17	300	2.49E-17	230	9.62E-20	260	4.90E-20
320	2.50E-17	352	2.04E-17	302	2.42E-17	235	7.61E-20	265	4.60E-20
321	2.46E-17	354	2.03E-17	304	2.36E-17	240	6.05E-20	270	4.10E-20
322	2.41E-17	355	2.02E-17	306	2.31E-17	245	4.88E-20	275	3.60E-20
323	2.36E-17	357	2.01E-17	309	2.23E-17	250	3.98E-20	280	2.90E-20
324	2.29E-17	359	1.99E-17	312	2.16E-17	255	3.23E-20	285	2.30E-20
325	2.24E-17	361	1.97E-17	314	2.10E-17	260	2.56E-20	290	1.70E-20
327	2.14E-17	363	1.96E-17	316	2.04E-17	265	2.11E-20	295	1.20E-20
328	2.06E-17	365	1.94E-17	318	1.98E-17	270	1.70E-20	300	8.10E-21
329	1.99E-17	366	1.93E-17	320	1.92E-17	275	1.39E-20	305	5.20E-21
330	1.91E-17	370	1.91E-17	321	1.87E-17	280	1.09E-20	310	3.20E-21
331	1.76E-17	372	1.89E-17	323	1.80E-17	285	8.63E-21	315	1.90E-21
332	1.63E-17	374	1.86E-17	325	1.76E-17	290	6.91E-21	320	1.10E-21
333	1.41E-17	377	1.85E-17	327	1.71E-17	295	5.51E-21	325	6.10E-22
334	1.27E-17	379	1.85E-17	329	1.68E-17	300	4.13E-21	330	3.70E-22
335	8.59E-18	381	1.82E-17	331	1.63E-17	305	3.13E-21	335	00E+00
336	7.24E-18	382	1.80E-17	334	1.62E-17	310	2.39E-21		
338	0	384	1.80E-17	337	1.61E-17	315	1.82E-21		

[a] The mechanisms used assume zero overall quantum yield, so the absorption cross sections do not affect the results. Absorption cross section data can be obtained from the Mainz spectral database (http://satellite.mpic.de/spectral_atlas/cross_sections/Halogen%20oxides/I%20oxides/OIO_Spietz(2005)_298K_391.85-659.55nmnm(1.3nm).txt.

compared to the competing unimolecular or O_2 reactions. Although reactions with $CF_3O\cdot$ are not expected to be important loss processes for VOCs in ambient atmospheres compared to their reaction with OH radicals, these reactions can be important sinks for $CF_3O\cdot$. In addition, because most of these reactions can ultimately lead to radical formation, can result in net radical propagation from the photolysis of CF_3I. This is analogous to the radical propagation caused by the formation of $CH_3\cdot$ radicals from the photolysis of CH_3I, though the mechanism is more complex.

VOC + $CF_3O\cdot$ reactions are represented in the model by adding a $CF_3O\cdot$ reaction for each SAPRC-11 model species used to represent reactive VOCs or VOC oxidation products. The products of these reactions are unknown, but are approximated by using the set of products used in the model for the corresponding OH reaction, with the H_2O formed in the abstraction reactions by OH being replaced by CF_3OH. The actual yields in abstraction for compounds with different types of abstractable H's may be somewhat different, and the products formed from the addition reactions may be considerably different (forming compounds with $-OCF_3$ substituents rather than -OH), but the effect of this approximation is assumed to be minor because the $CF_3O\cdot$ reaction is not a major loss process for the VOCs compared to their other reactions. In terms of CF_3I reactivity, the most factor affecting ozone impacts would be the total radical yield in the $CF_3O\cdot$ reaction, and the assumption that it is similar to that in the OH reaction is reasonable.

Rate constants have been measured for the reactions of $CF_3\cdot$ with a small number of VOCs, and representative data are shown on Table 4, along with rate constants for their reactions with OH radicals. Figure 1 shows plots of the measured $CF_3O\cdot$ rate constants against those for OH radicals, where it can be seen that the data for the non-aromatic compounds are well fit by

$$k(CF_3O\cdot + VOC) = 3.57 \times k(OH + VOC) \qquad (I)$$

This is used to estimate the rate constants for the reactions of $CF_3O\cdot$ with all the VOC model species, as discussed in Footnote 16 of Table 1. The data for benzene suggests that this may underestimate the rate constants for reactions of $CF_3O\cdot$ with aromatics, but the overprediction may not be as large for the higher aromatics that have significantly larger rate constants than benzene. In addition, most of the $CF_3O\cdot$ consumption in atmospheric modeling systems is due to the reactions of alkane model species, since the alkanes tend to be present in higher concentrations in the atmosphere than the aromatics. The rate constant estimate is considered to be the least uncertain for the alkanes.

The mechanism given in Table 1 has a number of uncertainties, and in some cases sensitivity calculations were conducted to determine their effects on reactivity predictions. As discussed below, probably the most important uncertainty in terms assessing whether these iodides should be regulated as ozone precursors appears to concern the photolysis of INO_2, which is an important reservoir for both iodine and NO_x. In our previous study (Carter, 2007) we did not find information on INO_2 photolysis and estimated a photolysis rate that is a factor of 10-25 higher than the range indicated by now-available data (see Table 2). Unfortunately, as discussed in Footnote 3 to Table 1, there is a discrepancy in the literature and the Mainz UV spectral database (Keller-Rudek et al, 2013) concerning these absorption cross sections, so the effects of this uncertainty were examined in the reactivity calculations discussed below.

Simulations of Methyl Iodide Chamber Experiments

Because we made significant changes to the iodine mechanism in this work relative to the version used in our previous study of methyl iodide (Carter, 2007), we evaluated it using the results of chamber experiments carried out by Carter (2007) to evaluate the previous mechanism for CH_3I. The experiments and modeling methods are described by Carter (2007), and that discussion is not reproduced here. The only significant change is the iodine mechanism, which is given in Table 1. Simulations were carried out

Table 4. Rate constants for the reactions of $CF_3O\cdot$ and OH radicals with VOCs at 300 K for compounds where CF_3O rate constants have been measured.

Compound	Rate constant [a]		
	OH	$CF_3O\cdot$	$CF_3O\cdot$ reference
Methane	6.68e-15	2.3e-14	NASA (2015)
Ethane	2.57e-13	1.3e-12	NASA (2015)
Propane	1.11e-11	4.8e-12	Kelley et al (1993) and Barone et al (1994)
2-methyl propane	7.20e-12	7.2e-12 2.8e-12	Kelley et al (1993) Barone et al (1994) (not used for estimates)
Ethene	8.52e-12	3.0e-11	Kelley et al (1993)
Propene	2.63e-11	7.2e-11	Kelley et al (1993)
Benzene	1.22e-12	3.0e-11	Kelley et al (1993)

[a] Rate constants in units of cm^3 $molec^{-1}$ s^{-1}. OH rate constants from evaluation of Calvert et al (2015).

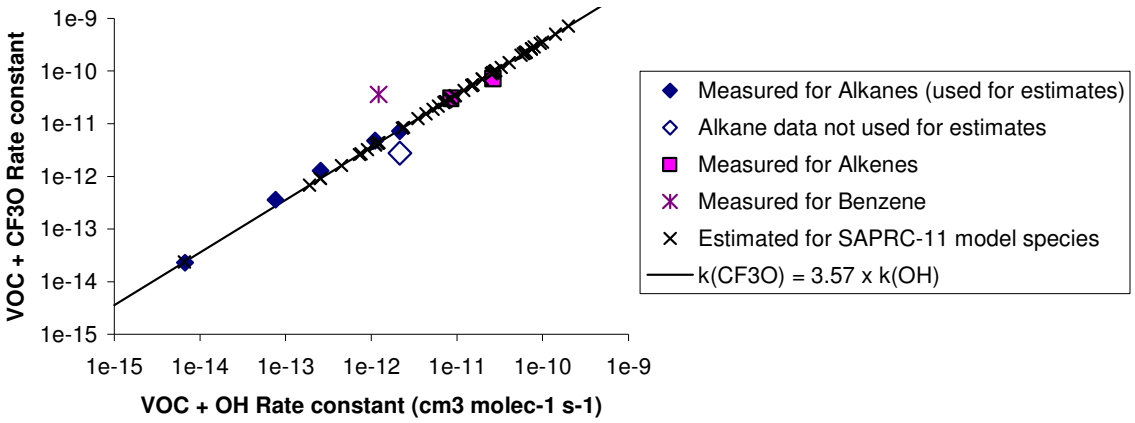

Figure 1. Plots of rate constants for the reactions of compounds and model species with CF3O· radicals against their rate constants for reactions with OH radicals. Rate constants for model species are estimated as discussed in the text.

using both the standard mechanism (using the NASA and IUPAC-recommended INO_2 absorption cross sections) and the mechanism assuming the high INO_2 photolysis rates as used by Carter (2007). The mechanisms were evaluated by comparing model predictions with experimental data for O_3, NO, and methyl iodide.

Scenarios and Reactivity Assessment Methods

The methods, scenarios, and reactivity scales that were used in this reactivity scale update are the same as employed previously for the SAPRC-99 and SAPRC-07 scales (Carter 2000, 2010a,b), and those

references should be consulted for detail. Briefly this is based on the methods and scenarios originally developed by Carter (1994a,b), with slight modifications in the averaging methods as described by Carter (2000). These are based on 39 single-day "base case" EKMA box model scenarios (EPA, 1984) derived by the EPA for assessing how various ROG and NO_x control strategies would affect ozone nonattainment in various areas of the country (Baugues, 1990). The conditions of these scenarios are summarized on Table 5, and more details concerning the modeling inputs are given by Carter (1994b).

The base case scenarios with the NO_x inputs as specified by Bauges (1990) were used to derive the updated "base case" reactivity scales. Because absolute and even relative impacts of VOCs on O_3 formation are highly dependent on NO_x conditions that are highly variable in the base case scenarios, scenarios with adjusted NO_x inputs were derived to obtain scales that are more representative of standard conditions of conditions of NO_x availability. These are as follows:

- The Maximum Incremental Reactivity (MIR) scale is derived from the scenarios where the NO_x inputs are adjusted to yield highest incremental reactivities of VOCs. This represents relatively high NO_x conditions where, by definition, O_3 is most sensitive to changes in VOC emissions.
- The Maximum Ozone Incremental Reactivity (MOIR) scale is derived from the scenarios where NO_x inputs are adjusted to yield highest maximum O_3 concentrations. This represents NO_x conditions that are most favorable to O_3 formation.
- The Equal Benefits Incremental Reactivity (EBIR) scale is derived from scenarios where NO_x inputs are adjusted so that the reduction in O_3 caused by reducing base ROG inputs are the same as those caused by changing total NO_x inputs by the same percentage. This represents the lowest NO_x conditions where controls of VOCs are at least as effective as controlling NO_x; since for lower NO_x levels NO_x controls are always more effective for reducing O_3.

Table 5 gives the NO_x levels that correspond to these various conditions of NO_x availability that were used to derive the MIR, MOIR, or EBIR scales. The incremental reactivities for those scales were averages of the incremental reactivities calculated for the 39 scenarios of the various types.

The incremental reactivity calculations were carried out by adding the amount of test compound such that the estimated amount reacted would be 0.05% the mole carbon of the base ROG input. (In the case of these iodides, 100% reaction was assumed for this purpose. This is an overestimate but is gave enough added iodide to have a non-negligible effect on calculated ozone.) The incremental reactivities were calculated change in final (i.e., maximum) O_3 concentrations in terms of total moles formed, divided by the moles of test compound or mixture added in the calculations. The incremental reactivities are then converted from mole to mass basis by using the molecular weights for O_3 and the test VOCs.

Table 5. Scenarios used for reactivity assessment, with selected inputs and calculated maximum O_3 for the base case, MIR, MOIR, and EBIR conditions.

Scenario	Max Height (km)	O3 Aloft (ppb)	ROG Input [a]	NOx Input [a]				Maximum O3 (ppb)			
				Base	MIR	MOIR	EBIR	Base	MIR	MOIR	EBIR
Atlanta, GA	2.1	63	11.8	1.62	3.40	2.26	1.58	175	149	183	174
Austin, TX	2.1	85	11.2	1.21	3.47	2.28	1.43	173	157	193	181
Baltimore, MD	1.2	84	16.8	3.26	4.47	2.92	1.70	328	251	331	301
Baton Rouge, LA	1.0	62	11.1	1.63	2.67	1.82	1.37	243	193	245	234
Birmingham, AL	1.8	81	12.8	1.85	4.89	3.25	2.08	242	208	267	250
Boston, MA	2.6	105	14.3	2.20	5.42	3.55	2.23	193	166	205	194
Charlotte, NC	3.0	92	7.5	0.96	4.19	2.74	1.97	139	140	166	162
Chicago, IL	1.4	40	25.0	2.15	6.07	4.08	2.63	290	250	335	310
Cincinnati, OH	2.8	70	17.3	2.71	5.41	3.53	1.96	199	161	204	186
Cleveland, OH	1.7	89	15.7	2.37	3.84	2.45	1.60	250	199	251	235
Dallas, TX	2.3	75	17.5	3.70	4.55	2.98	2.04	203	166	212	200
Denver, CO	3.4	57	29.3	4.64	6.30	4.14	2.66	204	165	206	193
Detroit, MI	1.8	68	17.3	2.54	4.91	3.22	1.78	242	187	247	224
El Paso, TX	2.0	65	12.3	1.86	2.83	1.84	1.31	182	149	182	174
Hartford, CT	2.3	78	10.7	1.28	4.01	2.58	1.53	169	151	190	177
Houston, TX	1.7	65	25.5	4.19	6.71	4.45	2.79	311	233	312	288
Indianapolis, IN	1.7	52	12.1	1.82	3.23	2.01	1.29	209	162	210	197
Jacksonville, FL	1.5	40	7.7	1.01	2.29	1.54	1.10	152	130	163	155
Kansas City, MO	2.2	65	9.1	1.28	3.14	2.03	1.10	154	130	163	149
Lake Charles, LA	0.5	40	7.0	0.94	2.09	1.45	1.04	293	239	318	302
Los Angeles, CA	0.5	100	23.1	3.04	4.69	3.12	2.14	587	424	587	552
Louisville, KY	2.5	75	13.7	2.48	4.55	2.93	1.96	208	166	210	199
Memphis, TN	1.8	58	14.9	2.20	4.83	3.22	2.01	227	181	239	222
Miami, FL	2.7	57	9.5	0.98	3.59	2.32	1.58	130	124	154	147
Nashville, TN	1.6	50	7.4	0.92	3.07	2.03	1.29	164	150	193	181
New York, NY	1.5	103	39.2	4.85	8.86	6.38	4.25	378	310	391	367
Philadelphia, PA	1.8	53	19.0	3.07	4.96	3.29	2.06	242	183	243	225
Phoenix, AZ	3.3	60	39.9	5.26	8.53	5.50	3.13	280	217	281	253
Portland, OR	1.6	66	6.2	0.96	2.21	1.37	0.95	162	133	169	161
Richmond, VA	1.9	64	16.4	2.65	4.90	3.22	1.79	237	184	241	218
Sacramento, CA	1.1	60	7.4	1.12	2.04	1.33	0.85	202	157	205	191
St Louis, MO	1.6	82	25.6	4.22	5.85	3.85	2.26	322	245	324	297
Salt Lake City, UT	2.2	85	10.7	1.26	3.27	2.08	1.21	183	160	196	182
San Antonio, TX	2.3	60	6.0	1.53	2.17	1.39	1.00	126	105	127	122
San Diego, CA	0.9	90	7.7	1.08	1.75	1.16	0.82	192	154	192	183
San Francisco, CA	0.7	70	25.0	5.24	4.36	2.97	2.19	260	364	477	453
Tampa, FL	1.0	68	7.9	1.81	2.44	1.66	1.21	226	179	227	217
Tulsa, OK	1.8	70	14.9	2.80	4.64	3.02	1.77	225	174	226	207
Washington, DC	1.4	99	13.5	2.54	4.53	3.03	1.89	279	218	283	264

[a] Initial + emitted anthropogenic VOC or total NO_x input, in units of millimoles C or N m^{-2}.

Results

Evaluation of the Mechanism Against Methyl Iodide Chamber Data

The ability of the Carter (2007) mechanism to predict the ozone impacts of methyl iodide was evaluated by comparing its predictions against results of environmental chamber experiments carried out as part of that study. Because the updated mechanism gave different reactivity results than the previous mechanism, it is appropriate to re-evaluate the mechanism against these chamber data. The results are shown on Figure 2 and Figure 3, which give experimental and calculated results for representative experiments. Four types of experiments were modeled, as discussed below:

Two CH_3I - NO_x experiments were carried out and the results are shown on Figure 2. Both models correctly predicted the initial NO oxidation and O_3 formation rates and the approximate rate of CH_3I consumption, though the 2007 mechanism somewhat underpredicted the NO oxidation rates at the middle stages of the experiments, suggesting somewhat better performance for the updated mechanism.

A number of CH_3I - CO - NO_x experiments were conducted, with CO being a simple surrogate for reactive VOCs. Results of representative experiments are shown also shown on Figure 2 -- the results for other experiments were similar. Again, both mechanisms correctly predicted the initial rates of NO and methyl iodide consumption and O_3 formation, though the updated mechanism somewhat overpredicted O_3 levels at the later stages of the experiments, though it performed better in simulating NO oxidation rates in the later stages of the experiment with the higher CH_3I levels.

Three incremental reactivity experiments were conducted where the effects of adding CH_3I to standard reactive VOC surrogate - NO_x experiments simulating atmospheric conditions were determined. Two were conducted with NO_x levels approximately half of those calculated to form maximum O_3 concentrations (MOIR/2) and one with higher NO_x levels estimated to give the highest incremental reactivities (MIR). The amount of CH_3I added was varied in the lower NO_x experiments. Again, the two

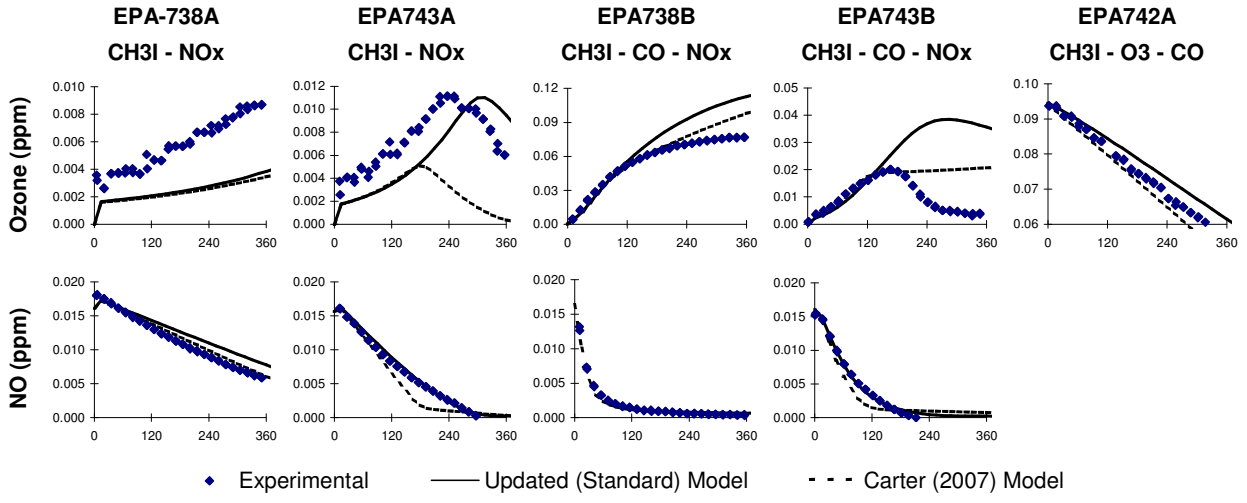

Figure 2. Experimental and calculated results of representative CH3I-NO_x, CH3I-CO-NO_x, and CH3I-CO-O_3 experiments from Carter (2007). Also includes results of model calculations updated for this work.

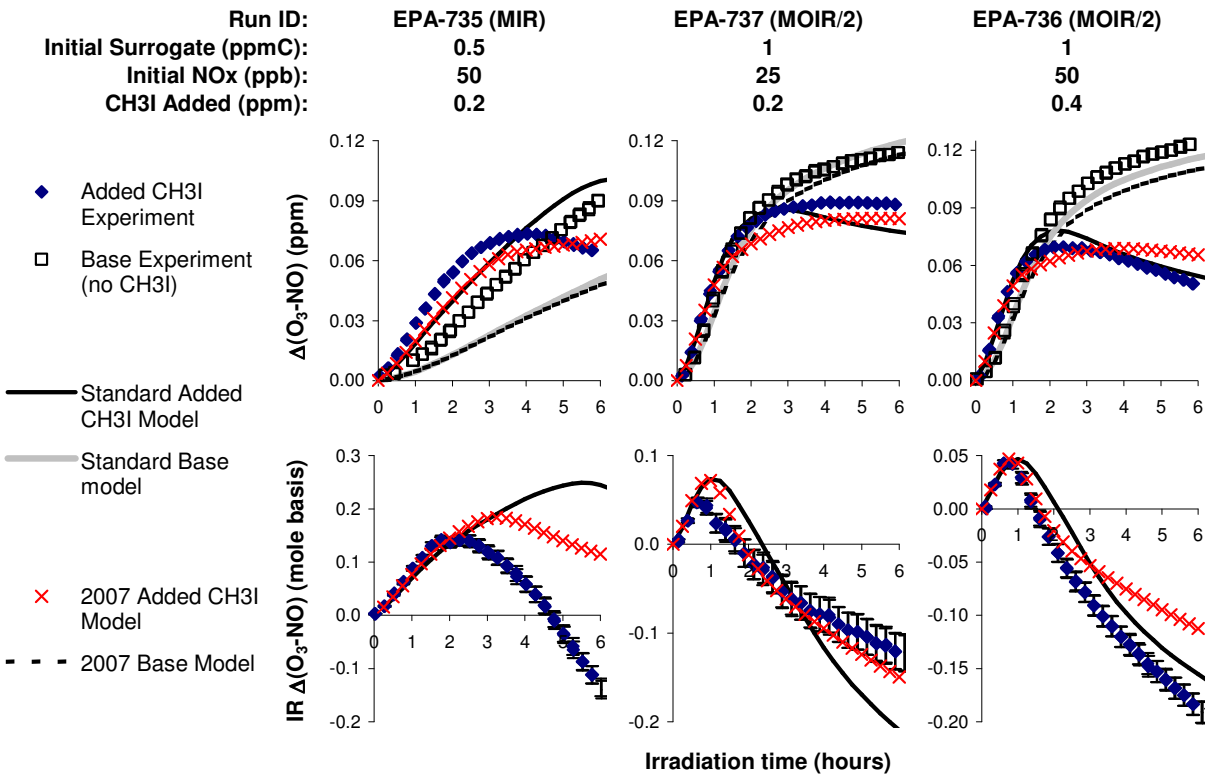

Figure 3. Experimental and calculated results of the incremental reactivity experiments with added methyl iodide from Carter (2007). Also includes model calculations updated for this work.

models give appropriate predictions of the effects of the added CH_3I on initial rates of NO oxidation and O_3 formation, but differed in the amount of O_3 inhibition predicted for the last half of the experiments. The updated mechanism predicted more inhibition, but the difference was not large compared to experimental variability for the two lower NO_x experiments. Both mechanisms predicted less inhibition by the end of the MIR experiment than observed experimentally, with the discrepancy being greater with the updated mechanism. However, the model underpredicted O_3 formation rates in the base case experiment, and that could contribute to the source of the discrepancy observed.

Overall, we conclude that the data are not sufficient to rule out or prefer the updates to the mechanism, particularly their predictions for MIR conditions, which are represented in the early stages of the reactivity experiments. Sensitivity calculations showed that changing the photolysis rates for INO_2 does not affect the simulations of initial NO oxidation and O_3 formation rates in the chamber experiments, so the experiments are not useful for assessing this uncertainty. The mechanisms differ primarily in their predictions of how much O_3 is inhibited in the later stages of the experiments, which affect primarily how much inhibition is calculated for lower NO_x conditions. Because the available chamber data do not strictly rule out or clearly prefer either mechanism, we use of the updated mechanism because it is more consistent with the current literature recommendations. However, it is still uncertain whether to use the reactivities calculated using the standard mechanism or with the higher INO_2 photolysis rates of Bröske (2000).

Calculated Atmospheric Reactivities

Methyl Iodide. The incremental reactivity results for methyl iodide are summarized on Table 6 and are plotted against relative NO_x inputs in the scenarios in Figure 4. Reactivity results for ethane, the informal low reactivity standard, are also shown, as well as reactivity results from Carter (2007). It can be seen that the updated mechanism gives similar results to the 2007 study in that it predicts that methyl iodide inhibits O_3 in the lower NO_x base case, MOIR, and EBIR scenarios, with the magnitude of the inhibition, and how it depends on NO_x conditions, being similar. However, the updated mechanism differs from the previous calculations in the higher NO_x (MIR) scenarios. In the previous study the inhibition by methyl iodide was calculated to become less as the NO_x is increased, but still to be an inhibitor in all the MIR scenarios, while for the updated mechanism the methyl iodide reactivities were calculated to be positive for most or all of the MIR scenarios, depending on the photolysis rate assumed for the INO_2 reaction. The positive reactivities were within the range of the reactivities of ethane for the standard mechanism using the NASA and IUPAC recommended INO_2 absorption cross sections, but were generally lower than ethane if the higher absorption cross sections reported by Bröske (2000) are employed.

Trifluoromethyl Iodide. The incremental reactivity results for ethane and trifluoromethyl iodide are summarized on Table 7 and are plotted against relative NO_x inputs in the scenarios in Figure 5. The results are qualitatively similar to those for methyl iodide (compare Figure 5 with Figure 4), with very similar magnitudes of negative reactivities for the lower NO_x scenarios, though with somewhat higher positive reactivities for the MIR scenarios. The magnitudes of the positive MIR reactivities were about 3 times higher than ethane on average if the standard mechanism is used, but overlap those of ethane if the higher INO_2 photolysis rates indicated by the data of Bröske (2000) are used. This represents an uncertainty range for our reactivity estimates for this compound.

In order to investigate the range of NO_x conditions where CH_3I and CF_3I may have positive reactivities or reactivities greater than ethane for the standard mechanisms, we also calculated incremental reactivities for scenarios with NO_x levels between those of MIR and MOIR conditions. These are designated "MIR-MOIR" for scenarios with NO_x levels halfway between those of MIR and MOIR, and "Near MIR" for scenarios with NO_x levels halfway between MIR-MOIR and MIR. The results are shown on the top right plot on Figure 4 and the right hand plot on Figure 5. It can be seen that the reactivities are negative for both iodides for both these scenarios, indicating that positive reactivities occur only under very high NO_x conditions near or above MIR levels. Figure 5 shows that only a slight reduction of NO_x from the MIR levels will result in reactivities of CF_3I becoming comparable or lower than those of ethane.

Discussion

Reactivity Results

The results of this study indicate that both methyl and trifluoromethyl iodide strongly inhibit O_3 formation in atmospheric scenarios most favorable for ozone formation and where O_3 formation is limited by the availability of NO_x. These represent the conditions of most regional models and the conditions used to derive the MOIR, EBIR, and most base case scales. On the other hand, the incremental reactivities of both compounds are predicted to be positive for the relatively high NO_x MIR scenarios. This is highly sensitive to NO_x levels, and if NO_x is reduced only slightly below MIR levels, and still above NO_x levels yielding maximum ozone, the reactivities become negative and both these iodides are ozone inhibitors. Therefore, both iodides are ozone inhibitors for all but the highest NO_x conditions.

The predicted reactivities relative to ethane in the high NO_x scenarios are strongly affected by the photolysis rate used for INO_2, which is highly uncertain. This sensitivity is attributed to the fact that

Table 6. Incremental reactivity results for ethane and methyl iodide. The iodide reactivities were calculated using the standard and the high INO_2 photolysis mechanisms.

Scenario	Incremental reactivities (grams O_3 per gram VOC emited)											
	Ethane				CH_3I - Standard Model				CH_3I - Faster INO2 Phot.			
	MIR	MOIR	EBIR	BASE	MIR	MOIR	EBIR	BASE	MIR	MOIR	EBIR	BASE
Average	0.24	0.18	0.13	0.17	0.27	-1.8	-2.3	-2.0	0.07	-2.0	-2.4	-2.2
St. Dev	0.07	0.06	0.04	0.04	0.14	0.3	0.3	0.6	0.14	0.3	0.3	0.6
Atlanta, GA	0.24	0.18	0.13	0.14	0.29	-1.63	-2.09	-2.07	0.07	-1.73	-2.17	-2.15
Austin, TX	0.27	0.21	0.15	0.14	0.20	-1.63	-2.09	-2.16	-0.04	-1.75	-2.17	-2.24
Baltimore, MD	0.23	0.17	0.11	0.21	0.41	-2.32	-2.95	-1.96	0.23	-2.53	-3.06	-2.25
Baton Rouge, LA	0.17	0.11	0.08	0.12	0.21	-1.52	-2.06	-1.79	0.07	-1.79	-2.24	-2.01
Birmingham, AL	0.33	0.24	0.18	0.19	0.44	-2.14	-2.76	-2.83	0.20	-2.35	-2.87	-2.94
Boston, MA	0.27	0.20	0.15	0.16	0.18	-1.69	-2.06	-2.06	-0.05	-1.81	-2.12	-2.12
Charlotte, NC	0.32	0.26	0.21	0.13	0.07	-1.64	-1.95	-2.13	-0.21	-1.70	-1.99	-2.16
Chicago, IL	0.21	0.14	0.10	0.09	0.33	-1.87	-2.48	-2.63	0.20	-2.20	-2.67	-2.80
Cincinnati, OH	0.31	0.24	0.17	0.22	0.34	-1.80	-2.32	-2.13	0.12	-1.92	-2.39	-2.21
Cleveland, OH	0.20	0.15	0.11	0.17	0.27	-1.97	-2.45	-2.04	0.07	-2.11	-2.53	-2.16
Dallas, TX	0.22	0.16	0.11	0.23	0.20	-1.31	-1.76	-0.61	0.05	-1.53	-1.91	-0.91
Denver, CO	0.18	0.12	0.09	0.15	0.43	-1.88	-2.44	-1.53	0.22	-1.98	-2.53	-1.69
Detroit, MI	0.28	0.21	0.15	0.20	0.36	-1.84	-2.37	-2.16	0.20	-2.02	-2.47	-2.28
El Paso, TX	0.18	0.13	0.09	0.14	0.33	-1.51	-2.00	-1.49	0.13	-1.63	-2.10	-1.61
Hartford, CT	0.30	0.23	0.17	0.18	0.20	-2.06	-2.54	-2.61	-0.07	-2.14	-2.59	-2.66
Houston, TX	0.26	0.18	0.13	0.19	0.34	-1.75	-2.33	-1.89	0.20	-2.04	-2.49	-2.14
Indianapolis, IN	0.27	0.19	0.14	0.20	0.34	-2.06	-2.55	-2.22	0.12	-2.18	-2.64	-2.32
Jacksonville, FL	0.25	0.16	0.12	0.12	0.30	-1.70	-2.14	-2.21	0.07	-1.83	-2.23	-2.29
Kansas City, MO	0.33	0.25	0.18	0.22	0.24	-1.83	-2.31	-2.25	-0.01	-1.90	-2.37	-2.30
Lake Charles, LA	0.18	0.11	0.08	0.11	0.00	-2.09	-2.61	-2.70	-0.15	-2.47	-2.85	-2.91
Los Angeles, CA	0.08	0.05	0.04	0.08	-0.06	-1.46	-2.04	-1.54	-0.14	-1.88	-2.31	-1.95
Louisville, KY	0.34	0.25	0.18	0.24	0.30	-1.95	-2.38	-2.19	0.04	-2.06	-2.45	-2.27
Memphis, TN	0.31	0.20	0.14	0.17	0.45	-2.14	-2.65	-2.60	0.24	-2.32	-2.75	-2.70
Miami, FL	0.29	0.21	0.16	0.11	0.33	-1.75	-2.17	-2.38	0.06	-1.83	-2.22	-2.44
Nashville, TN	0.43	0.31	0.22	0.18	0.41	-2.07	-2.59	-2.77	0.11	-2.19	-2.67	-2.85
New York, NY	0.15	0.08	0.06	0.08	0.39	-2.25	-2.71	-2.64	0.23	-2.54	-2.83	-2.78
Philadelphia, PA	0.25	0.17	0.12	0.18	0.41	-1.87	-2.41	-2.01	0.26	-2.09	-2.52	-2.19
Phoenix, AZ	0.25	0.19	0.13	0.20	0.32	-1.71	-2.32	-1.79	0.12	-1.90	-2.44	-1.97
Portland, OR	0.27	0.20	0.16	0.18	0.22	-1.88	-2.25	-2.24	-0.02	-1.96	-2.31	-2.29
Richmond, VA	0.27	0.20	0.14	0.20	0.52	-2.21	-2.85	-2.54	0.32	-2.37	-2.94	-2.65
Sacramento, CA	0.21	0.15	0.12	0.20	-0.03	-1.93	-2.44	-2.20	-0.23	-2.10	-2.55	-2.33
St Louis, MO	0.20	0.14	0.09	0.17	0.39	-1.96	-2.54	-1.68	0.24	-2.18	-2.67	-1.97
Salt Lake City, UT	0.28	0.23	0.16	0.18	0.27	-1.74	-2.27	-2.23	0.00	-1.81	-2.32	-2.28
San Antonio, TX	0.25	0.19	0.15	0.22	0.14	-1.15	-1.45	-0.99	-0.04	-1.26	-1.52	-1.12
San Diego, CA	0.11	0.07	0.06	0.10	-0.03	-1.23	-1.65	-1.36	-0.12	-1.48	-1.80	-1.58
San Francisco, CA	0.07	0.05	0.04	0.10	0.07	-1.57	-2.26	0.13	-0.02	-2.00	-2.54	0.12
Tampa, FL	0.22	0.14	0.10	0.19	0.22	-1.83	-2.32	-1.53	0.02	-2.07	-2.47	-1.83
Tulsa, OK	0.29	0.20	0.14	0.21	0.36	-2.06	-2.52	-2.18	0.15	-2.19	-2.59	-2.29
Washington, DC	0.26	0.19	0.14	0.19	0.28	-1.93	-2.45	-2.22	0.10	-2.17	-2.57	-2.39

Table 7. Incremental reactivity results for ethane and trifluoromethyl iodide. The iodide reactivities were calculated using the standard and the high INO_2 photolysis mechanisms.

Scenario	Incremental reactivities (grams O_3 per gram VOC emitted)											
	Ethane				CF_3I - Standard Model				CF_3I - Faster INO2 Phot.			
	MIR	MOIR	EBIR	BASE	MIR	MOIR	EBIR	BASE	MIR	MOIR	EBIR	BASE
Average	0.24	0.18	0.13	0.17	0.71	-2.7	-3.4	-2.9	0.32	-2.8	-3.4	-3.0
St. Dev	0.07	0.06	0.04	0.04	0.22	0.4	0.5	0.9	0.22	0.5	0.5	0.9
Atlanta, GA	0.24	0.18	0.13	0.14	0.56	-2.24	-2.87	-2.84	0.15	-2.26	-2.92	-2.88
Austin, TX	0.27	0.21	0.15	0.14	0.45	-2.31	-2.94	-3.05	0.01	-2.35	-2.99	-3.11
Baltimore, MD	0.23	0.17	0.11	0.21	1.02	-3.52	-4.32	-3.07	0.63	-3.64	-4.38	-3.28
Baton Rouge, LA	0.17	0.11	0.08	0.12	0.68	-2.40	-3.10	-2.75	0.36	-2.59	-3.22	-2.89
Birmingham, AL	0.33	0.24	0.18	0.19	0.99	-3.13	-3.89	-3.99	0.48	-3.21	-3.94	-4.05
Boston, MA	0.27	0.20	0.15	0.16	0.42	-2.38	-2.85	-2.85	-0.02	-2.42	-2.88	-2.88
Charlotte, NC	0.32	0.26	0.21	0.13	0.07	-2.19	-2.60	-2.90	-0.34	-2.19	-2.61	-2.93
Chicago, IL	0.21	0.14	0.10	0.09	0.95	-3.11	-3.90	-4.11	0.64	-3.40	-4.04	-4.25
Cincinnati, OH	0.31	0.24	0.17	0.22	0.70	-2.55	-3.25	-2.98	0.26	-2.59	-3.31	-3.01
Cleveland, OH	0.20	0.15	0.11	0.17	0.64	-2.91	-3.58	-3.00	0.20	-2.95	-3.62	-3.03
Dallas, TX	0.22	0.16	0.11	0.23	0.62	-2.06	-2.68	-0.99	0.30	-2.22	-2.78	-1.33
Denver, CO	0.18	0.12	0.09	0.15	0.78	-2.66	-3.46	-2.24	0.34	-2.67	-3.53	-2.28
Detroit, MI	0.28	0.21	0.15	0.20	0.88	-2.75	-3.45	-3.14	0.53	-2.85	-3.52	-3.22
El Paso, TX	0.18	0.13	0.09	0.14	0.67	-2.18	-2.86	-2.16	0.26	-2.21	-2.91	-2.18
Hartford, CT	0.30	0.23	0.17	0.18	0.58	-2.70	-3.35	-3.46	0.09	-2.68	-3.36	-3.49
Houston, TX	0.26	0.18	0.13	0.19	0.92	-2.82	-3.57	-2.98	0.60	-3.04	-3.69	-3.17
Indianapolis, IN	0.27	0.19	0.14	0.20	0.78	-2.86	-3.59	-3.09	0.34	-2.90	-3.64	-3.12
Jacksonville, FL	0.25	0.16	0.12	0.12	0.69	-2.31	-2.89	-2.98	0.26	-2.33	-2.93	-3.02
Kansas City, MO	0.33	0.25	0.18	0.22	0.57	-2.37	-3.05	-2.96	0.14	-2.36	-3.09	-2.98
Lake Charles, LA	0.18	0.11	0.08	0.11	0.77	-3.25	-3.91	-4.02	0.43	-3.55	-4.06	-4.16
Los Angeles, CA	0.08	0.05	0.04	0.08	0.55	-2.77	-3.82	-2.92	0.40	-3.47	-4.19	-3.58
Louisville, KY	0.34	0.25	0.18	0.24	0.60	-2.70	-3.30	-3.02	0.12	-2.70	-3.31	-3.02
Memphis, TN	0.31	0.20	0.14	0.17	1.05	-3.00	-3.64	-3.56	0.59	-3.05	-3.68	-3.60
Miami, FL	0.29	0.21	0.16	0.11	0.58	-2.32	-2.88	-3.21	0.14	-2.31	-2.89	-3.26
Nashville, TN	0.43	0.31	0.22	0.18	0.91	-2.71	-3.39	-3.66	0.38	-2.72	-3.42	-3.71
New York, NY	0.15	0.08	0.06	0.08	0.85	-3.73	-4.23	-4.15	0.49	-4.01	-4.35	-4.28
Philadelphia, PA	0.25	0.17	0.12	0.18	0.99	-2.81	-3.48	-2.97	0.65	-2.93	-3.55	-3.07
Phoenix, AZ	0.25	0.19	0.13	0.20	0.81	-2.65	-3.54	-2.78	0.40	-2.78	-3.64	-2.89
Portland, OR	0.27	0.20	0.16	0.18	0.56	-2.50	-3.03	-3.01	0.13	-2.48	-3.03	-3.02
Richmond, VA	0.27	0.20	0.14	0.20	1.11	-3.15	-3.97	-3.55	0.68	-3.19	-4.03	-3.58
Sacramento, CA	0.21	0.15	0.12	0.20	0.71	-2.61	-3.35	-2.99	0.29	-2.67	-3.40	-3.03
St Louis, MO	0.20	0.14	0.09	0.17	0.96	-3.12	-3.89	-2.76	0.61	-3.28	-4.00	-3.00
Salt Lake City, UT	0.28	0.23	0.16	0.18	0.51	-2.36	-3.10	-3.05	0.05	-2.34	-3.12	-3.07
San Antonio, TX	0.25	0.19	0.15	0.22	0.35	-1.62	-2.03	-1.40	0.03	-1.67	-2.07	-1.47
San Diego, CA	0.11	0.07	0.06	0.10	0.45	-1.99	-2.56	-2.17	0.23	-2.21	-2.68	-2.35
San Francisco, CA	0.07	0.05	0.04	0.10	0.61	-2.93	-4.02	0.71	0.41	-3.55	-4.30	0.68
Tampa, FL	0.22	0.14	0.10	0.19	0.71	-2.74	-3.35	-2.35	0.28	-2.86	-3.43	-2.55
Tulsa, OK	0.29	0.20	0.14	0.21	0.82	-2.88	-3.48	-3.03	0.37	-2.90	-3.52	-3.04
Washington, DC	0.26	0.19	0.14	0.19	0.83	-2.95	-3.60	-3.31	0.43	-3.11	-3.68	-3.41

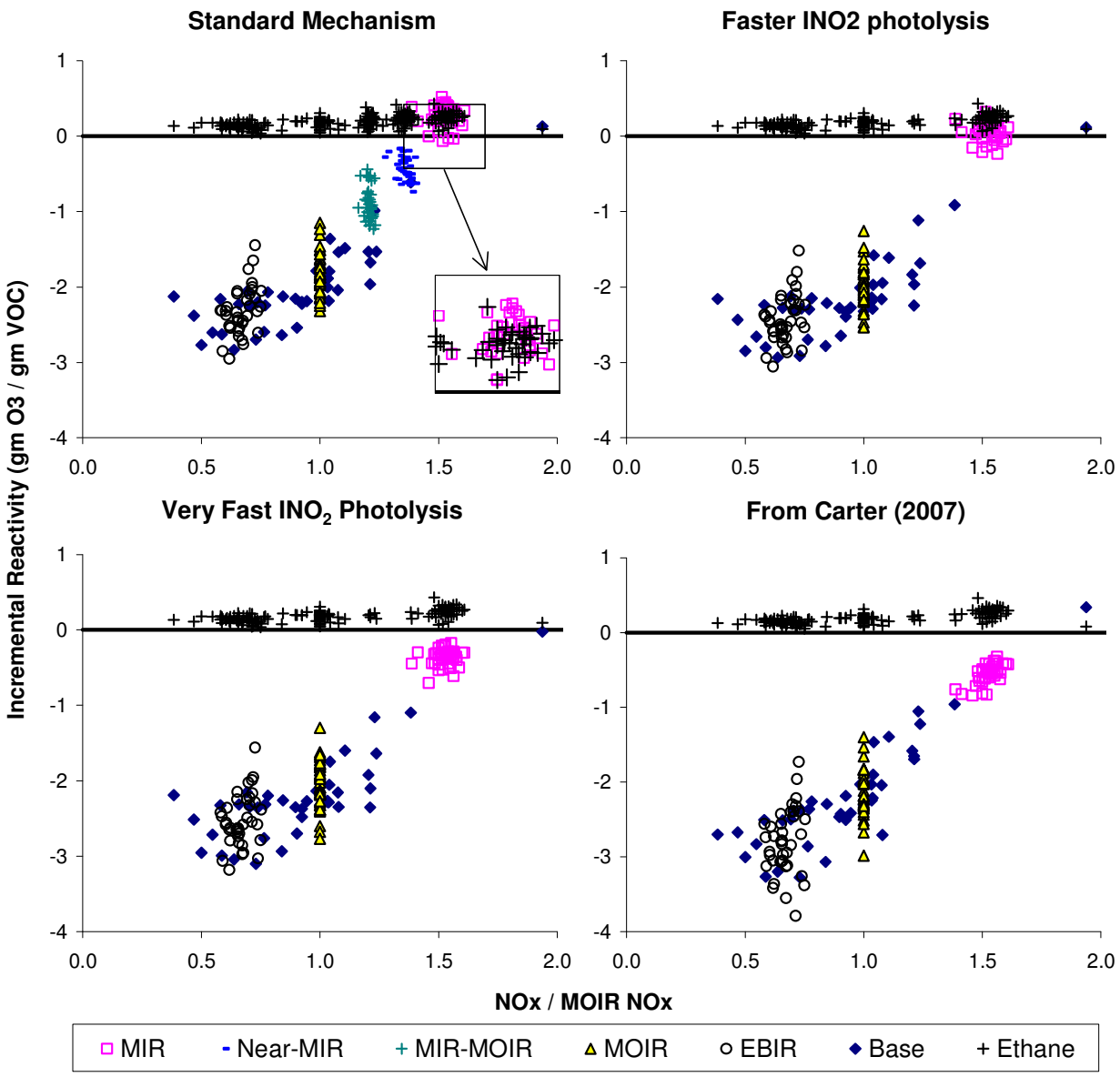

Figure 4 Plots of incremental reactivities of ethane and methyl iodide for the various types of scenarios against the ratio of NO_x inputs to NO_x levels giving the maximum ozone concentrations. The methyl iodide reactivities were calculated using three different assumptions for the photolysis of INO2, and also with the mechanism of Carter (2007)..

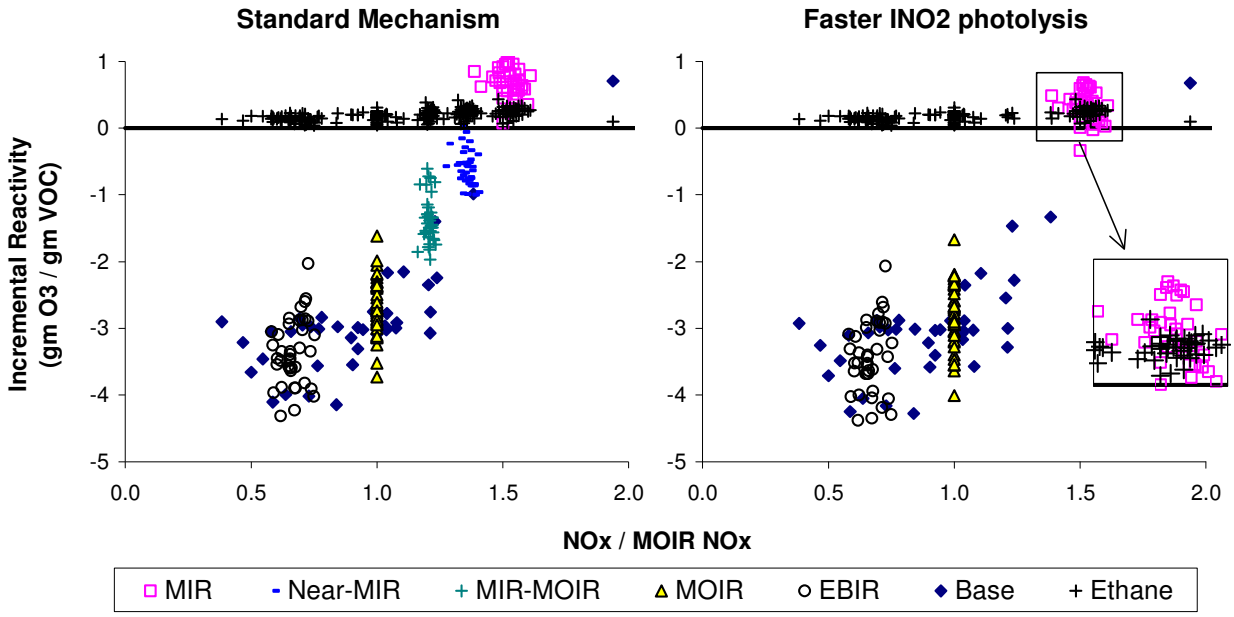

Figure 5. Plots of incremental reactivities of ethane and trifluoromethyl iodide for the various types of scenarios against the ratio of NO_x inputs to NO_x levels giving the maximum ozone concentrations. The trifluoromethyl iodide reactivities were calculated using two different assumptions for the photolysis of INO_2.

formation and photolysis of INO_2 serves as an important but temporary NO_x sink when iodides are photolyzed in the presence of NO_x. The rate of O_3 formation in high NO_x scenarios is determined primarily by overall radical levels, which are inhibited when NO_x levels are increased, so temporary NO_x sinks such as formation of INO_2,will have the effect of reducing the rate of this termination process and therefore temporarily increasing radical levels, causing positive incremental reactivities. However, NO_x is required for O_3 to form, so sufficiently large NO_x sinks will cause negative reactivities under lower NO_x conditions, as is observed for these iodides.

With regard to exemptions, the main issue is the reactivity relative to ethane. This is only an issue for MIR conditions for these iodides, since they are calculated to be inhibitors if NO_x is reduced even slightly below that which gives maximum incremental reactivity (MIR). This is not as much of a concern for methyl iodide because its MIR reactivities are calculated to be less than or comparable to ethane regardless of the INO_2 photolysis rates used. On the other hand, the calculated MIR reactivities of CF_3I are uniformly higher than those for ethane if the INO_2 photolysis rate at the low end of its uncertainty range is used, but are comparable to those of ethane if the photolysis rate is at the high end of the range. Therefore, what is assumed about the photolysis rate of INO_2 affects whether INO_2 is predicted to have higher MIR reactivities than ethane.

The uncertainty concerns a discrepancy between reported INO_2 absorption cross sections from the only published measurement, as discussed in Footnote 3 to the mechanism listing in Table 1. There is a factor of 2.5 discrepancy between the NASA recommended absorption cross sections (which in turn are based on a earlier IUPAC [2000] evaluation) for INO_2 and those on the Maintz database attributed to the thesis of Bröske (2000), which is apparently the only experimental measurement considered in the evaluations. The NASA (2015) write-up notes the discrepancy in the Mainz database but adopts the IUPAC evaluation without comment. The IUPAC write-up does not state why the reported values are

different than those on the Mainz database for Bröske (2000), but does say that the values are preliminary because the write-up and analysis was not completed (at that time, which was also 2000). They cited a 1999 version of the Bröske thesis, which is presumably superceded by Bröske (2000). Therefore, it is not clear why there is a factor of 2.5 difference, and it could be that the actual photolysis rate is 2.5 times faster. It could be that Bröske found some reason to change the calibration factor after the IUPAC review was completed but before he submitted the results to the Mainz database. Therefore, we suspect that the "Faster INO_2 photolysis" mechanism, which predicts MIR values for CF_3I that are comparable to ethane, is more likely to be correct. The reactivities predicted by the "Standard" mechanism can be considered reasonable upper limits.

Use of Reactivity Results for Exemptions

Decisions to exempt compounds based on negligible ozone impacts should be based on considerations of all atmospheric conditions where ground level ozone is a problem and can be reduced by VOC controls. Ideally this should be done using comprehensive 3D models designed to represent the full distribution of ozone episodes in regions that would be affected by the regulations, but this is not currently practical. Instead the approach has been to use either considerations of reaction rates to determine if it is possible for the compound to react fast enough to possibly have a reactivity greater than ethane, and if so develop or estimate mechanisms for the compounds and conduct box model calculations of reactivities for a wide variety of scenarios. If the reaction rates are such that the compound cannot be more reactive than ethane under any conditions, or if the calculated box model reactivities are always less than ethane, then it is reasonable to exempt the compound on the basis of low reactivity.

Note that the types of box model reactivity scenarios carried out here and used to derive current SAPRC reactivity scales are significant simplifications of conditions in actual airsheds, where transport and aging of pollutants are significant, and NO_x levels vary depending on locations of air parcels relative to the sources. Because of this, 3D models such as CMAQ (2019) need to be used to represent conditions of specific airsheds. It is argued that use of the simplified box models of Carter (1994a,b) gives an appropriate estimate for a general reactivity measure for positively reactive compounds because relative reactivities of positively reactive compounds are not as sensitive to scenario conditions, allowing use of simplified scenarios for general estimation purposes. Therefore, use of more comprehensive 3D models is not considered necessary if the box model calculations give consistent results for the variety of scenarios used.

The issue is somewhat less straightforward if the reactivity relative to ethane varies significantly with atmospheric conditions in both sign and magnitude. In those cases, and one must consider the net effects of the emissions on the airshed as a whole. Use of a single scale such as MIR is not appropriate because of this variability. The MIR scale was proposed (Carter, 1994) and adopted (CARB 1993, 2000, 2016) for use in reactivity-based regulatory applications requiring use of a single scale because it gave the most consistent results for positively reactive compounds, reflected conditions where O_3 is most sensitive to VOC emissions, and gave good correlations to ozone exposure and reactivity scales calculated using 3D models (e.g., Hakami et al, 2004). However, these arguments are not applicable to ozone inhibitors, especially for compounds such as CF_3I whose reactivities vary in both sign and magnitude.

In the case of CF_3I we have a compound that may (or may not) have reactivities greater than ethane under MIR NO_x conditions but are inhibitors everywhere else. Note that MIR conditions are actually relatively rare in the atmosphere, reflecting highly urbanized or industrial conditions near NO_x sources, not the downwind areas where highest O_3 concentrations tend to occur. It is also not clear that it is appropriate to regulate as an ozone precursor a compound that inhibits O_3 under all but the highest NO_x conditions, especially if the high NO_x positive reactivities are primarily due to additional NO_x sinks caused by the reactions of the compound. NO_x is required for O_3 formation and is the major factor

affecting the maximum amounts of O_3 that can be formed, so NO_x sinks are ultimately beneficial as far as reducing O_3 formation is concerned. It is likely that the net effect of increasing CF_3I emissions would cause O_3 reductions throughout an airshed. However, his would need to be verified using 3D calculations to be certain.

It should be noted that if CF_3I were exempted, it would not be the first exempted compound that has MIR values that are greater than those for ethane. Both acetone (EPA, 2009; Carter et al, 1993) and 2-amino-2-methyl-1-propanol (AMP) (Federal Register 2014; Carter, 2012) were known to have higher MIRs than ethane but were exempted on the basis of lower or negative reactivities under MOIR and other conditions. AMP is of particular interest because its reactivity characteristics are remarkably similar to CF_3I, despite the quite different chemistry involved. This is shown on Figure 6, which slows plots of AMP and ethane reactivities against NO_x levels, as calculated by Carter (2012). It can be seen that, like CF_3I, many of the MIR reactivities of AMP are higher than ethane, though the compound inhibits O_3 in the lower NO_x scenarios. Although the mechanisms are quite different, the reason for the results are the same -- there are strong NO_x sinks in both mechanisms. This was determined to be a sufficient reason to exempt AMP, and an exemption for CF_3I would be consistent with this.

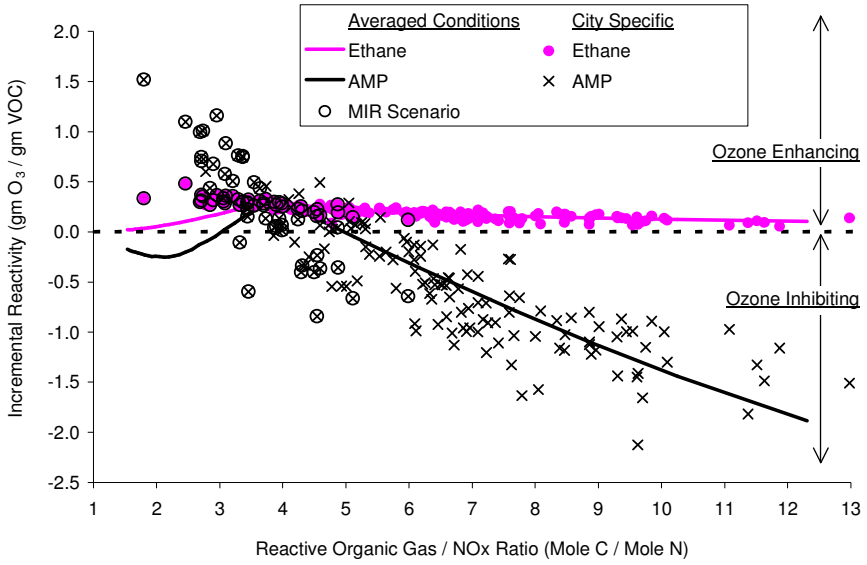

Figure 6. Plots of incremental reactivities of 2-amino-2-methyl-1-propanol (AMP) and ethane against the reactive organic gas / NO_x ratio for the averaged conditions and city-specific scenarios. The scenarios used to derive the MIR values are circled (Figure taken from Carter, 2012 without modification.)

Acknowledgements

This work was funded by a consulting contract with Honeywell International Inc. Dr. Dimitrios Papanastasiou of Honeywell corporation contributed significantly to the literature search that led to the mechanism updates, by reviewing versions of the mechanism, and by helpful discussions. However, the opinions and conclusions in this report are entirely those of the author.

References

Barone, S.B., A. A. Turnispeed, and A. R. Ravishankara (1994): "Kinetics of the Reactions of the CF_3O Radical with Alkanes," J. Phys. Chem. 98, 4602-4608, https://pubs.acs.org/doi/abs/10.1021/j100068a020

Baugues, K. (1990): "Preliminary Planning Information for Updating the Ozone Regulatory Impact Analysis Version of EKMA," Draft Document, Source Receptor Analysis Branch, Technical Support Division, U. S. Environmental Protection Agency, Research Triangle Park, NC, January.

Bloss, W.J., D.M. David M. Rowleym R.A, Cox, and R.L. Jones (2001): "Kinetics and Products of the IO Self-Reaction," J. Phys. Chem. A, 105, 7840-7854, https://doi.org/10.1021/jp0044936.

Bröske, R. (2000) "Kinetische und spektroskopische Untersuchungen von Nitrylhalogeniden, Halogennitriten und Halogennitraten", Ph. D. thesis, University of Wuppertal, Germany, 2000. Available in German from the University of Wuppertal web site.

Calvert, J. G., J. J. Orlando, W. R. Stockwell, and T. J. Wallington (2015): "The Mechanisms of Reactions Influencing Atmospheric Ozone," Oxford University Press, New York.

Carter, W. P. L. (1994a): "Development of Ozone Reactivity Scales for Volatile Organic Compounds," J. Air & Waste Manage. Assoc., 44, 881-899.

Carter, W. P. L. (1994b): "Calculation of Reactivity Scales Using an Updated Carbon Bond IV Mechanism," Report Prepared for Systems Applications International Under Funding from the Auto/Oil Air Quality Improvement Research Program, April 12.

Carter, W. P. L. (2000): "Documentation of the SAPRC-99 Chemical Mechanism for VOC Reactivity Assessment," Report to the California Air Resources Board, Contracts 92-329 and 95-308, May 8. Available at http://www.cert.ucr.edu/~carter/absts.htm#saprc99.

Carter, W. P. L. (2007): "Investigation of the Atmospheric Ozone Impacts of Methyl Iodide," Final Report to the Arysta LifeScience Corporation, Contract UCR-07041867, July 31. Available at https://intra.engr.ucr.edu/~carter/absts.htm#ch3irep.

Carter, W. P. L. (2010a): "Development of the SAPRC-07 Chemical Mechanism and Updated Ozone Reactivity Scales," Final report to the California Air Resources Board Contract No. 03-318. January 27. Available at www.cert.ucr.edu/~carter/SAPRC.

Carter, W. P. L. (2010b): "Development of the SAPRC-07 Chemical Mechanism," Atmospheric Environment, 44, 5324-5335.

Carter, W. P. L. (2012): "Atmospheric Ozone Reactivity Estimates for 2-Amino-2-Methyl-1-Propanol," College of Engineering Center for Environmental Research and Technology (CE-CERT), available on request from carter@cert.ucr.edu.

Carter, W. P. L. (2013): "SAPRC Atmospheric Chemical Mechanisms and VOC Reactivity Scales," web site at https://intra.engr.ucr.edu/~carter/SAPRC/, last updated September 14.

Carter, W. P. L. and G. Heo (2012): "Development of Revised SAPRC Aromatics Mechanisms," Report to the California Air Resources Board Contracts No. 07-730 and 08-326, April 12, 2012. Available at http://www.cert.ucr.edu/~carter/absts.htm#saprc11.

Carter, W. P. L. and G. Heo (2013): "Development of Revised SAPRC Aromatics Mechanisms," Atmos. Environ. 77, 404-414.

CARB (1993): "Proposed Regulations for Low-Emission Vehicles and Clean Fuels -- Staff Report and Technical Support Document," California Air Resources Board, Sacramento, CA, August 13, 1990. See also Appendix VIII of "California Exhaust Emission Standards and Test Procedures for 1988 and Subsequent Model Passenger Cars, Light Duty Trucks and Medium Duty Vehicles," as last amended September 22, 1993. Incorporated by reference in Section 1960.

CARB (2000): "Initial Statement of Reasons for the Proposed Amendments to the Regulation for Reducing Volatile Organic Compound Emissions from Aerosol Coating Products and Proposed Tables of Maximum Incremental Reactivity (MIR) Values, and Proposed Amendments to Method 310, 'Determination of Volatile Organic Compounds in Consumer Products'," California Air Resources Board, Sacramento, CA, May 5.

CARB (2016): "Reactivity-Based VOC Regulations," California Air Resources Board web page at https://www.arb.ca.gov/research/reactivity/regulation.htm. Last updated September, 2010. Last updated January, 2016.

CMAQ (2019): "Community Modeling and Analysis System", https://www.cmascenter.org/cmaq/, accessed September. See also "CMAQ: The Community Multiscale Air Quality Modeling System," https://www.epa.gov/cmaq, last updated August 30.

Dillon, T.J., M. E.Tucceri, and J. N. Crowley (2006): "Laser induced fluorescence studies of iodine oxide chemistry. Part II.w The reactions of IO with CH3O2, CF3O2 and O3," Phys. Chem. Chem. Phys., 2006, 5185-5198, DOI: 10.1039/b611116e

Dimitriades, B. (1999): "Scientific Basis of an Improved EPA Policy on Control of Organic Emissions for Ambient Ozone Reduction," J. Air & Waste Manage. Assoc. 49, 831-838

EPA (1984): "Guideline for Using the Carbon Bond Mechanism in City-Specific EKMA," EPA-450/4-84-005, February.

EPA (2019): "Code of Federal Regulations. 40 CFR Part 51.100. Available at https://www.ecfr.gov/cgi-bin/text-idx?rgn=div8&node=40:2.0.1.1.2.3.8.1.

Federal Register (2014): "Air Quality: Revision to the Regulatory Definition of Volatile Organic Compounds—Exclusion of 2-amino-2-methyl-1-propanol (AMP)," Vol. 79, No. 59, 17037-17043, March 27

Gómez Martín, T.C., Gálvez, O, Baeza-Romero, M.T., Ingham, T., Plan, J.M.C., Blitz, M. A. (2013). "On the mechanism of iodine oxide particle formation," Phys.Chem. Chem. Phys., 2013, 15, 15612-15622, DOI: 10.1039/c3cp51217g.

Hakami, A., R. A. Harley, J. B. Milford, M. T. Odman and A. G. Russell (2004): "Regional, Three-Dimensional Reactivity Assessment of Organic Compounds," Atmos. Environ. 38, 121-134.

IUPAC (2000): IUPAC Subcommittee on Gas Kinetic Data Evaluation, "Evaluated Kinetic and Photochemical Data for Atmospheric Chemistry: Supplement VIII, Halogen Species," J. Phys. Chem. Ref. Data, 29, 167-266. http://dx.doi.org/10.1063/1.556058.

IUPAC (2019): IUPAC Subcommittee on Gas Kinetic Data Evaluation for Atmospheric Chemistry, "Evaluated Kinetic and Photochemical Data". Web Version. Available at http://iupac.pole-ether.fr. Latest data sheets dated July, 2019.

Keller-Rudek, H., Moortgat, G. K., Sander, R., and Sörensen, R. (2013): The MPI-Mainz UV/VIS spectral atlas of gaseous molecules of atmospheric interest, Earth Syst. Sci. Data, 5, 365–373, (2013), DOI: 10.5194/essd-5-365-2013.

Kelly, C,J., Treaty, and H,W. Sidebottom (1993): Rate constants for the reaction of CF30 radicals with hydrocarbons at 298 K," Chem Phus Lett. 207, 498-503, https://doi.org/10.1016/0009-2614(93)E1463-Q

NASA (2015): "Chemical Kinetics and Photochemical Data for Use in Atmospheric Studies. Evaluation Number 18" JPL Publication 15-10, Jet Propulsion Laboratory, Pasadena, California, Ocrober. Available at https://jpldataeval.jpl.nasa.gov/.

RRWG (1999a): "VOC Reactivity Policy White Paper," Prepared by the Reactivity Research Work Group Policy Team, October 1. Available at http://www.narsto.org/section.src?SID=10.

RRWG (1999b): "VOC Reactivity Science Assessment", Prepared by the Reactivity Research Working Group Science Team, May. Available at http://www.narsto.org/section.src?SID=10.

Saiz-Lopez,A. , R.P. Fernandez, C. Ordóñez2, D.E. Kinnison, J.C. Gómez Martín, J.-F. Lamarque, and S. Tilmes (2014): "Iodine chemistry in the troposphere and its effect on ozone, Atmos. Chem. Phys., 14, 13119-13143, doi:10.5194/acp-14-13119-2014

Spietz, P., J.C. Gomez Martin, and J.P. Burrows (2005): "Spectroscopic studies of the I_2/O_3 photochemistry. Part 2. Improved spectra of iodine oxides and analysis of the IO absorption spectrum," J. Photochem. Photobiol. A: Chem. 176, 50-67 (2005); DOI: 10.1016/j.jphotochem.2005.08.023

Tucceri, M.E., D. Holscher, A. Rodriguez, T.J. Dillon and J.N. Crowley (2005): "Absorption cross section and photolysis of OIO," Phys. Chem. Chem. Phys., 2006, 834-846, DOI: 10.1039/b512702e

Venecek, M. A., C. Cai, A. Kaduwelab, J. Aviseb,e, W. P.L. Carterc (2018): "Analysis of SAPRC16 chemical mechanism for ambient simulations," Atmos Environ, 192, 136-150.